STABLE REVERSE BIAS OR INTEGRATED BYPASS DIODE IN HIP-MWT+ SOLAR CELLS BASED ON DIFFERENT INDUSTRIAL REAR PASSIVATION

Tadeo Schweigstill[1], Alma Spribille[1], Jonas D. Huyeng[1], Florian Clement[1], Stefan W. Glunz[1,2]
Fraunhofer Institute for Solar Energy Systems ISE
[1] Heidenhofstraße 2, 79110 Freiburg, Germany
Telefon: +49 761 4588-0, Fax: +49 761 4588-9000, E-Mail: info@ise.fraunhofer.de
[2] Department for Sustainable Systems Engineering, University Freiburg
Emmy-Noether-Straße 2, 79110 Freiburg, Germany
Telefon: 0761 / 203 – 96783, E-Mail: info@inatech.uni-freiburg.de

The Metal Wrap Through+ (HIP-MWT+) solar cell is based on the PERC concept but features two additional electrical contacts, namely the Schottky contact between p-type Si bulk and Ag n-contact and the metal-insulator-semiconductor (MIS) contact on the rear side of the cell below the n-contact pads. To prevent hotspots under reverse bias, both contacts shall either restrict current flow or allow a homogenous current flow at low voltage. In this work we present both options. First the stable reverse bias characteristics up to -15 V with a MIS contact using industrially manufactured SiON passivation and second, an integrated by-pass diode using AlO_X as insulator in the passivation stack allowing current flows at approximately $V_{rev} = -3.5$ V depending on the chosen screen-print paste. The examined Schottky contacts break down at around $V_{rev} = -2.5$ V. Reverse bias testing of the cells proof a solid performance of the cells under reverse bias and an average conversion efficiency of $\eta = 21.2$ % (AlO_X) and $\eta = 20.7$ % (SiON), respectively.

Key words: MWT Solar Cell, PERC, Silicon Solar Cell, Passivation, back contact

1 INTRODUCTION

The passivated emitter and rear cell (PERC) [1] technology is now the standard technology in industrial production [2]. An advanced version of the PERC concept is the High-Performance Metal Wrap Through+ (HIP-MWT+) cell where only one additional process step (drilling of vias) is required to create a PERC with p- and n-contact located on the rear side of the cell [3]. This back-contact configuration results in several intuitive benefits such as a rear side module interconnection and reduced front side shading.

However, wrapping the metal through the Si bulk and placing the external n-contact on the rear also introduces new electrical contacts, namely the Schottky contact between p-type Si bulk and Ag n-contact in the vias and the metal-insulator-semiconductor (MIS) contact on the rear side of the cell below the n-contact pads. A schematic cross-section of the cell and the resulting electrical contacts are illustrated in **Figure 1**.

These additional contacts offer the following customization potential. If the contacts are designed for electrical insulation, a cell with a stable reverse bias characteristic is created, comparable to a regular PERC. This means that reverse current flow under partial shading in the module is restrained and thus hotspots are prevented. A standard module integration of such cells should then pass the IEC certification.
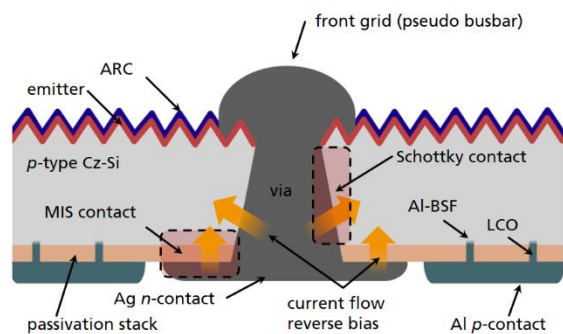

Figure 1: Cross sections of HIP-MWT + cell. Showing location of Schottky and MIS contact and potential current flows under reverse bias (yellow arrows).

On the other hand, one can also exploit the contacts by designing dielectric layers which insulate under forward bias but allow a current flow through the cell under reverse bias across a large area. This way an integrated bypass diode is built into the cell with only little additional production effort. This means that the module assembly is significantly simplified since no parallel bypass diodes are required in the module and a single shaded cell is not leading to an outage of a whole cell-string, which would reduce the power output of a typical module by 33 percent.

To find suitable passivation stacks for the insulating and conducting properties in the MIS contacts, different passivation principles can be compared. First, a chemical passivation using SiO_2 appears suitable to create an isolating passivation stack. Second, a passivation based on the electrical field effect using AlO_X seems appropriate to function as a rectifying contact [4].

2 EXPERIMENTAL

For the experimental realization of different contacts, two solar cell precursor types are used. The precursors are sourced from different industrial partners, after the front and rear surface passivation has been applied. Both precursor types are made from p-type Cz-Si and all passivation stacks are deposited using Plasma Enhanced Chemical Vapor Deposition (PECVD). The first stack is relying on the chemical passivation with a total thickness of $d \approx 160$ nm consisting of a hydrogenated siliconoxynitride (SiON) stack ($d \approx 75$ nm) capped with SiN_X ($d \approx 85$ nm) [5]. The second stack, relying on the electrical field effect passivation with a total thickness of $d \approx 150$ nm, is consisting of an AlO_X stack ($d < 20$ nm) and again a SiN_X capping ($d \approx 130$ nm) [6]. The metal side in the Schottky and MIS contact is created by a screen-printing process. While formally referred to as Ag, it is no pure metal due to the additives in the screen-printing paste. As the screen-printing paste contributes to the electric contacts, two screen-printing pastes with slightly different compositions were applied. The following manufacturing of test structures and solar cells was carried out using industrial production equipment located at the PV-TEC laboratory of Fraunhofer ISE [7].

Based on the described precursors, two types of dedicated test structures are manufactured: First a set of test structures to reveal the individual *IV*-characteristics of the MIS and Schottky contact, which show the reverse bias breakdown of the two contacts for different precursors and passivation stacks. Therefore, the different precursor types were metallized via screen printing. While the frontside (no anti-reflection coating) was fully metalized with an Al-paste to create a well-conducting contact, the rear side was metallized with circular Ag-pads with diameters between $\varnothing = 0.5$ mm and $\varnothing = 2.5$ mm. To create test samples with MIS as well as Schottky contacts, 50 % of the test samples had the rear side passivation stack removed prior to metallization. After metallization, all samples were then submitted to a contact firing process at $T_{peak} = 850$ °C. The samples were measured using an industrial 4-Point-Probe *IV*-setup. Two measurement pins were contacted on the front and two on the rear side, thus the *IV*-characteristics of the contacts were determined. The front side contact was proven to be ohmic, hence not influencing the measured rectifying behavior of Schottky and MIS contact. For the measurements, voltage sweeps from -15 V to $+15$ V were conducted with a step size of 10 mV, a delay of 50 ms and a current compliance of 1000 mA. Additionally, ten consecutive voltage sweeps from 10 V to -10 V were performed (interjacent cooldown phases of 5 s) to show the *IV*-characteristics of the contacts over several reverse bias cycles.

Second, a set of test structures for lock-in thermography imaging (LIT) of the spatial breakdown was processed. These samples ran through the same process steps as the regular HIP-MWT+ cells (see paragraphs below). However, to further investigate the contact characteristics using LIT, the rear side metallization layout and the underlying LCOs were adapted. Instead of the regular rear side *n*-pads, a pad geometry variation was carried out with circular pads reaching from $\varnothing = 2$ mm to $\varnothing = 20$ mm each with one via in the center of the pad. After screen printed metallization, the samples were contact fired at $T_{peak} = 850$ °C and measured in a commercial solar cell analysis system (LOANA, pv-tools [8]). Each sample was measured seven times with set voltages from -1 V to -10 V, a LI-frequency of 18.75 Hz and a measurement duration of up to 300 s for low voltages.

Finally, HIP-MWT+ cells with a 6 pseudo-busbar layout in M2 format were manufactured on the industrial precursors with the named industrial process tools at Fraunhofer ISE. The HIP-MWT+ cells were manufactured in five process steps.

In the first process step the precursors were processed in an industrial laser system (ILS500X, Innolas Systems [9]). Here, the HIP-MWT+ cells receive local contact openings (LCOs) ($\varnothing = 40$ µm, pitch of 500 µm) and 48 vias ($\varnothing_{rear} = 148$ µm, $\varnothing_{front} = 100$ µm) across the whole cell. In the following rear side metallization process, the via-filling is achieved by a controlled suction process of the vacuum chuck [10]. The following screen printing of the Al contact and front side grid were realized in parallel to standard PERC processes using an automated screen printer (XH2, ASYS TECTON GmbH). After contact firing the cell performance was measured in a commercial solar cell analysis system (customized, h.a.l.m. Elektronik GmbH [11]). Additionally, the manufactured cells were used for reverse bias cycling to demonstrate the long-term stability of the cells and the electrical contacts for 20 consecutive cycles at -15 V (Forward bias at standard testing conditions for 100 ms and reverse bias for 40 ms with a compliance current of $I_{rmax} = -0.5$ A).

3 RESULTS AND DISCUSSION

3.1 *IV*-Characteristics of Schottky and MIS Contact

The Schottky contact on the AlO$_X$ based precursor (AlO$_X$ removed) breaks at initial reverse bias at approximately $V_{rev} = -1.5$ V to $V_{rev} = -2.5$ V depending on the applied screen-printing paste as shown in **Figure 2**. The Schottky contact for the SiON based precursor (SiON removed) breaks at approximately $V_{rev} = -1$ V [4]. The different breakdown voltages for the Schottky contacts both consisting of *p*-type Si and Ag (with paste additives) is related to the varying bulk doping of the precursor material. While the SiON based precursor has lower bulk doping of $N \approx 7.3\times10^{15}$ atoms/cm^3, the AlO$_X$ based precursor has a significantly higher bulk doping of $N \approx 1.7\times10^{16}$ atoms/cm^3, resulting in a reduced width of the Schottky barrier and thus a lower breakdown voltage.

Over several reverse bias cycles the breakdown voltage is decreasing for all measured samples independent from the precursor and utilized screen-printing paste. The effect is the strongest between the first and second bias with the most significant right shift of the *IV*-characteristic. For all following reverse bias cycles the effect is incrementally decreasing, meaning that the contact tends to stabilize over several cycles. The increased contact formation can be explained by the percolation model which has been reported in electrical contacts before [12].

The same effect is observed even more significantly for the MIS contact using the AlO$_X$ passivation as insulator as shown in **Figure 2**. Furthermore, the choice of the screen-print paste seems to have a major impact on the *IV*-characteristics of the MIS and Schottky contact. While the contacts using paste 1 shows a constantly increasing
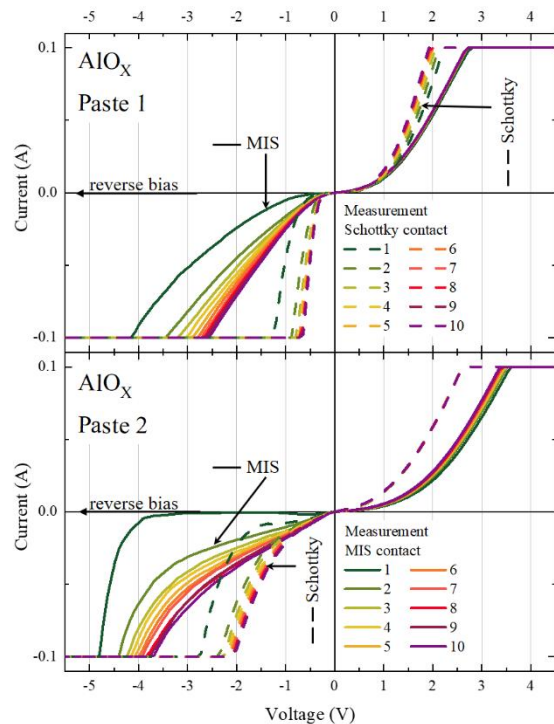

Figure 2: Repeated *IV*-characteristics of quantitative test structures for Schottky and MIS contact of the AlO$_X$ based precursor with two different screen-print pastes.

reverse current towards higher voltages, the *IV*-characteristics using of the contact using paste 2 shows a more distinct knee in the curve during the voltage sweep at negative bias. This means that the reverse current increase is more sudden and thus the breakdown is more abrupt especially for the first bias.

We suggest that the different breakdown behaviors originate from different paste ingredient. The abrupt breakdown of the contacts using paste 2 are closer to the *IV*-characteristic of an ideal diode and suggest that the present contact is more homogenous than contacts using paste 1 with the creeping breakdown. The paste ingredient responsible for the inhomogeneous contact formation is the glass fritt [13] which has a weight content of approximately $5 - 10$ wt% in paste 1 and approximately $0 - 1$ wt% in paste 2.

The MIS contact using the SiON passivation is not showing any breakdown in the range from -15 V to $+15$ V independent from the chosen screen-print paste. The described chemical passivation is thus considered stable under reverse bias in a regular solar cell assembly.

3.2 Lock-in Thermography Imaging Results

The Lock-in Thermography (LIT) images of the dedicated test structures confirm the findings of the *IV*-characteristics for the Schottky contact and MIS contact on cell level. As shown in **Figure 3,** the SiON based precursors only allows a small current flow under reverse bias (-3 V to -10 V) at the vias where the Schottky contact is located. The MIS contact underneath the *n*-pads is completely restricting the current flow.

The LIT images for the AlOx based precursor show a different behavior. At a reverse bias voltage of $V_{rev} = -3$ V a current flow is essentially observed at the vias as shown in **Figure 3**. At a voltage of $V_{rev} = -5$ V accessory currents are flowing from the *n*-pads to the *p*-type Si bulk, meaning that the MIS contact's breakdown voltage is exceeded. At $V = -10$ V the currents are spread more homogenously among the whole MIS contact across the whole test wafer.

The LIT image at $V = -10$ V is also revealing a higher current flow at the *n*-pad edges (ring structure). The increased current flow at the edges is correlated to an increase pad height. We suggest that the increased paste application at the edges leads to a higher glass frit concentration resulting in an increased contact formation. Therefore, the mass of applied paste during screen-printing seems suitable, among other parameters, to manipulate the breakdown voltage of the MIS contact.
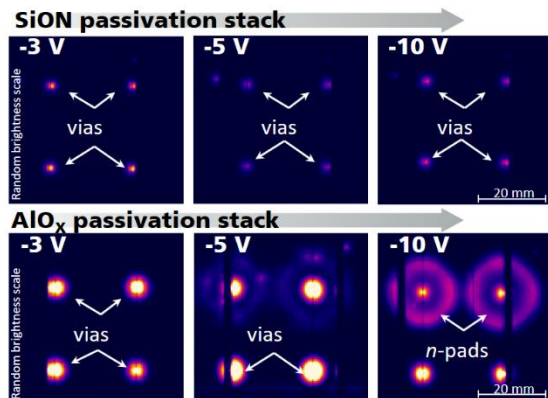

Figure 3: LIT images of test structures at different voltages, showing the spatially resolved reverse current for the SiON and AlOx based precursor.

3.4 Cell Results and Degradation by Reverse Bias Cycling

The cell results of the manufactured HIP-MWT+ cells suffer from technical issues during the screen-printing process which caused narrowing in the fingers and thus an increased series resistance. However, the cells still showed a solid performance with an average conversion efficiency $\eta = 21.2$ % for the the AlOx based precursor and $\eta = 20.7$ % for the the SiON based precursor (20 cells per group). The deviation in the conversion efficiency is related to several precursor parameters such as base resistivity (AlOx based precursor 0.94 ± 0.03 Ω cm and SiON based precursor 1.97 ± 0.14 Ω cm), and passivation. The open-circuit voltage (V_{oc}) and short-circuit current (j_{sc}) are reflecting the differences in the precursor parameters and can be obtained from **Table I.**

In terms of long-term stability, the HIP-MWT+ cells show a solid performance for the first 20 cycles. While the cells with the SiON passivation stack are not affected by the reverse cycling, the cells using the AlOx passivation stack show a slight decrease in the conversion efficiency of $\Delta_{\eta abs} = 0.2$ %, reducing the average conversion efficiency from $\eta_{abs} = 21.2$ % to $\eta_{abs} = 21.0$ %.

Table I: Average cell results for HIP-MWT+ cells. Per cell group 20 cells were measured.

Rear passivation group	η (%)	V_{OC} (mV)	j_{sc} (mA/cm²)	*FF* (%)
AlOx initial	21.2	671.4	40.2	78.65
AlOx 20th cycle	21.0	671.9	40.1	77.64
SiON initial	20.7	665.5	39.6	78.71
SiON 20th cycle	20.7	666.2	39.6	78.76

Furthermore, the HIP-MWT+ cells using the AlOx passivation show acceptable heat dissipation under reverse bias with a power dissipation < 40 W at $V_{rev} = -10$ V. This is still significantly below the upper limit of the 80 W limit a module encapsulation is able to cope with without being damaged [14]. This leads to the conclusion that the HIP-MWT+ cells using the SiON passivation stack, as well as the ones using the AlOx passivation stack are suited for module assembly.

4 CONCLUSION

The *IV*-measurements of the Schottky contacts show a breakdown in the test structures under reverse bias at voltages between $V_{rev} = -1.0$ V to $V_{rev} = -2.5$ V depending on several factors such as the Si bulk doping (precursor material) and the screen-printing paste. Furthermore, a decrease in the breakdown voltages is observed when several reverse biases are applied. This percolation effect is most significant with the first reverse bias and gradually decreasing with each following applied voltage.

The MIS contact using the AlOx passivation breaks in a similar manner as the Schottky contacts at slightly higher reverse voltages, while the MIS contact using the SiON passivation shows no breakdown down to $V_{rev} = -15$ V.

The LIT images on cell-level confirm the findings from the *IV*-characteristic. The cells using the AlOx passivation allow a reverse current from via metallization to Si bulk at small voltages ($V_{rev} \approx -5$ V). At higher voltages the current also flows through the MIS contact. The repeated reverse bias testing on cell level leads to marginal cell degradation resulting in a decrease of conversion efficiency of approximately $\Delta_{\eta abs} = 0.2$ % (from $\eta_{abs} = 21.2$ % to $\eta_{abs} = 21.0$ %).

Cells using the SION passivation stack only allow small nonhazardous currents from via metallization to Si bulk and no current through the MIS contact even at higher voltages ($V_{rev} = -10$ V). The repeated reverse bias testing for these cells is not significantly affecting the cell performance. However, further data is required to determine long-term effects on the MIS and Schottky contacts which must therefore be subject of future research activities.

REFERENCES

[1] A. W. Blakers, A. Wang, A. M. Milne, Appl. Phys. Lett. 55, 13 (1989)

[2] ITRPV, International Technology Roadmap for Photovoltaic (ITRPV) - Results 2018, 2019.

[3] B. Thaidigsmann, Ph.D. thesis, University of Tübingen, 2013

[4] T. Schweigstill, A. Spribille, J. D. Huyeng, F. Clement, S. W. Glunz, Proceedings 38th European Photovoltaic Solar Energy Conference and Exhibition, 2CO.10.2, (2021)

[5] C. Schwab, M. Hofmann, R. Heller, J. Seiffe, J. Rentsch, R. Preu, physica status solidi (a) 210, 11 (2013)

[6] P. Saint-Cast, D. Kania, M. Hofmann, J. Benick, J. Rentsch, R. Preu, Applied Physics Letters, 95, 15 (2009)

[7] Fraunhofer ISE, Neue Technologien und Solarzellen-wirkungsgrade aus dem Fraunhofer ISE PV-TEC press release 26, 2019.

[8] pv-tools GmbH, [Online]. Available: http://www.pv-tools.de/products/loana-system/loana-start.html. [Accessed 17 06 2021].

[9] InnoLas Solutions, [online]. Available: https://www.innolas-solutions.com/laser-machines-products/linexo-linear-table-laser-machine/. [Accessed 17 06 2021].

[10] E. Lohmüller, B. Thaidigsmann, S. Werner, F. Clement, A. Wolf, D. Biro, R. Preu, Proceedings 27th European Photovoltaic Solar Energy Conference and Exhibition, 2AO.2.6, (2012)

[11] h.a.l.m. Elektronik GmbH, [online]. http://www.halm.de/en/products/production/solar-cell.html [Accessed 17 06 2021].

[12] Z. Gingl, C. Pennetta, L. B. Kiss, L. Reggiani, In Semicond. Sci. Technol. 11, 12 (1996)

[13] Hilali, M. M., Sridharan, S., Khadilkar, C., Shaikh, A., Rohatgi, A., & Kim, S. (2006). Effect of glass frit chemistry on the physical and electrical properties of thick-film Ag contacts for silicon solar cells. Journal of electronic materials, 35(11), 2041-2047.

[14] I. Geisenmeyer, F. Fertig, W. Warta, S. Rein, M. C. Schubert, (2012): Proceedings 27th European Photovoltaic Solar Energy Conference. Frankfurt, pp. 870–874.